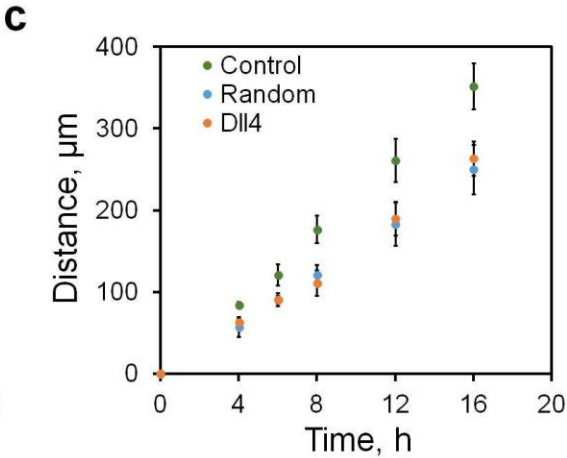
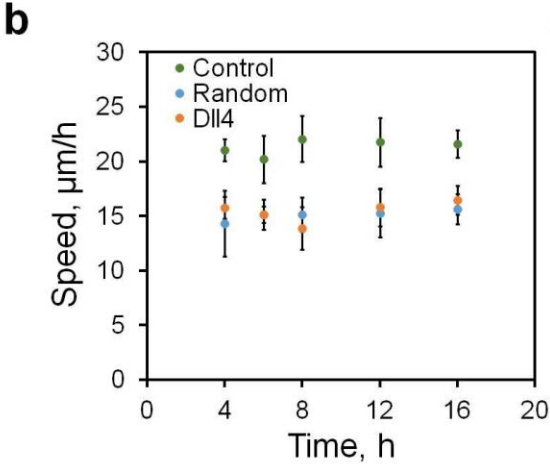
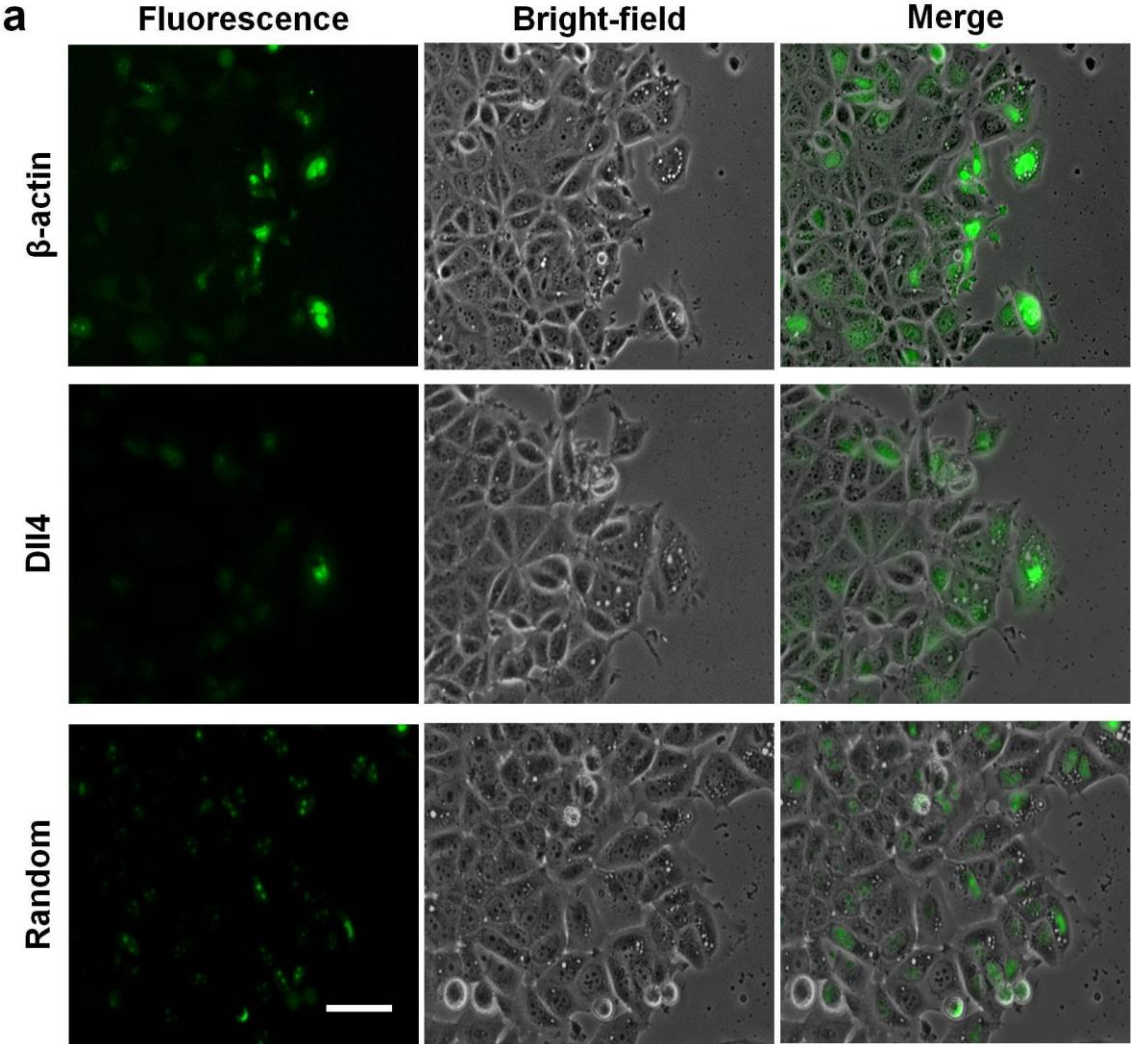
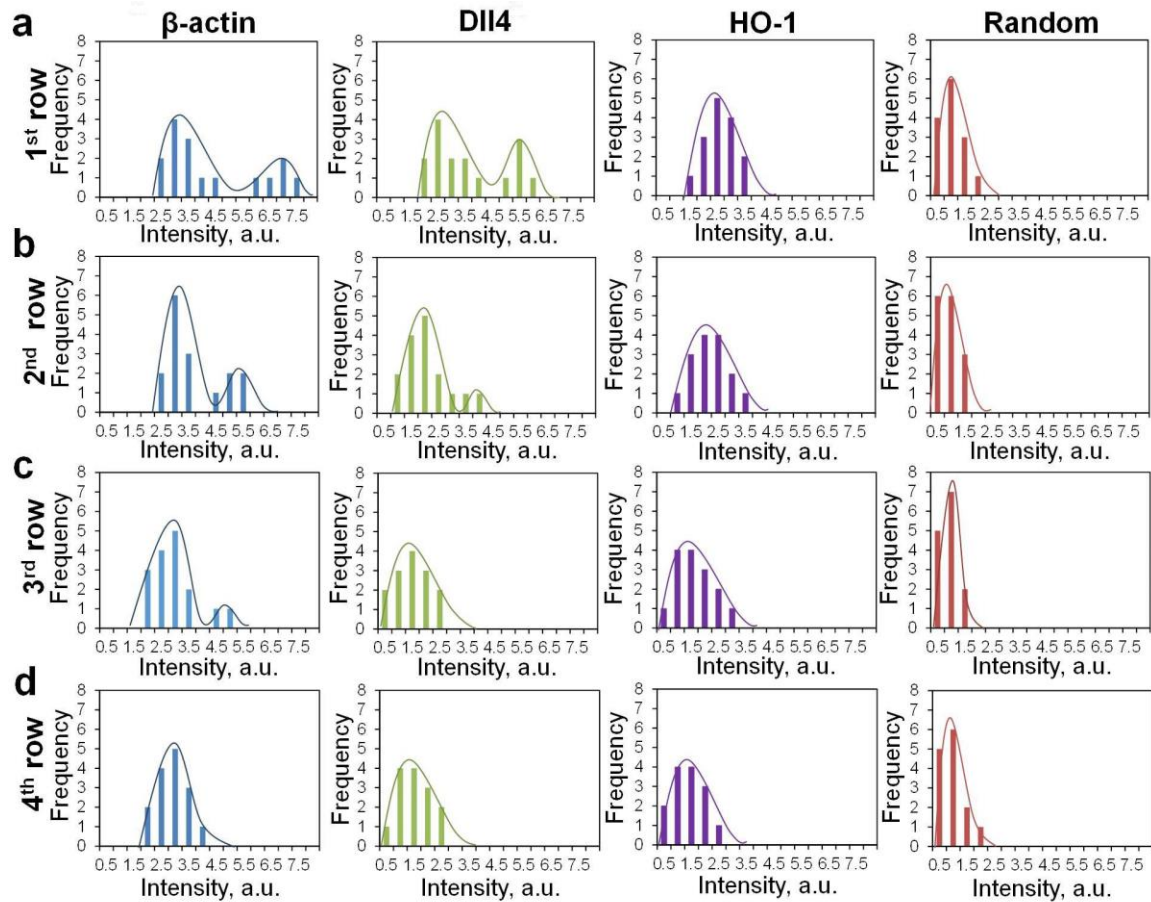


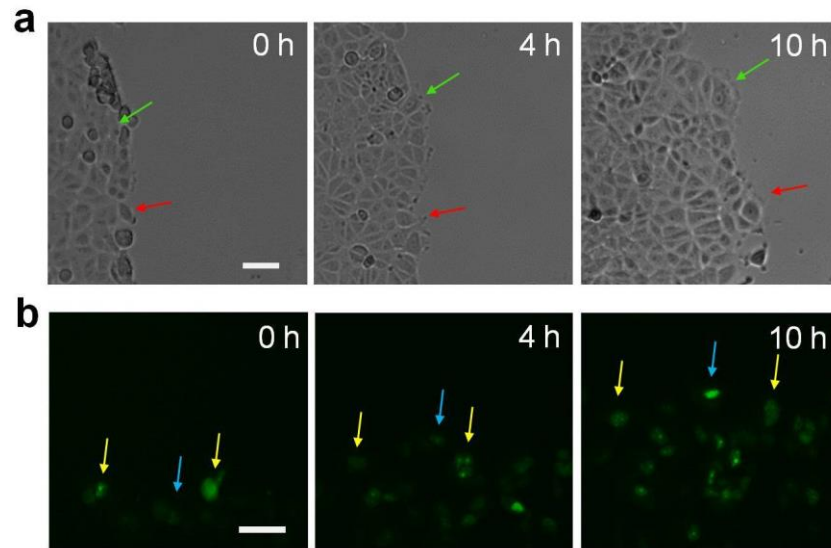
Supplementary Figures



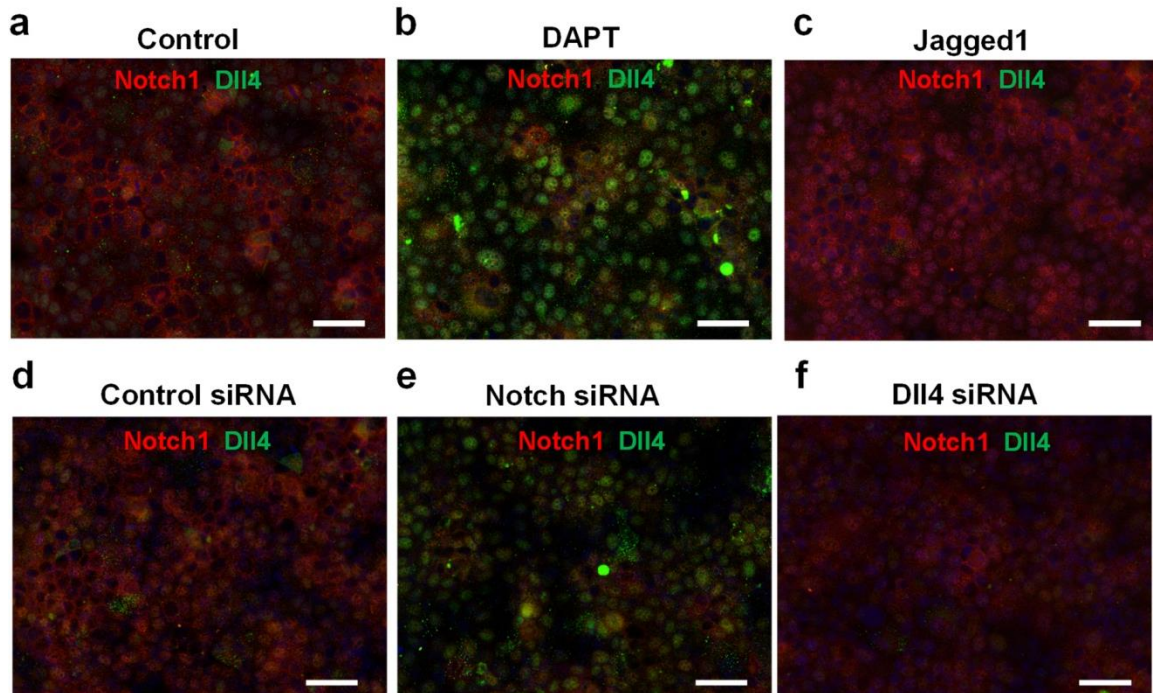
Supplementary Figure 1. Single cell gene expression analysis during collective cell migration. (a) Florescence and bright-field images of MCF7 cells transfected with dsLNA probes targeting β -actin mRNA, Dll4 mRNA, and random sequence near the leading edge. The model wounds were created by scratching cell monolayers with sterilized 1000 μ l pipette tips. Images are merged to correlate the cell morphology with gene expression in leader cells. Images are representatives of four independent experiments. Scale bar, 25 μ m. (b-c) Effects of dsLNA probes on cell migration. Migration speed (b) and distance (c) of cells transfected with Dll4 mRNA and random probes. Control represents cells without probe transfection. No statistically significant difference was found between Dll4 and random probes ($P > 0.05$; paired Student's t-test). Data are expressed as mean \pm s.e.m. (n=3).



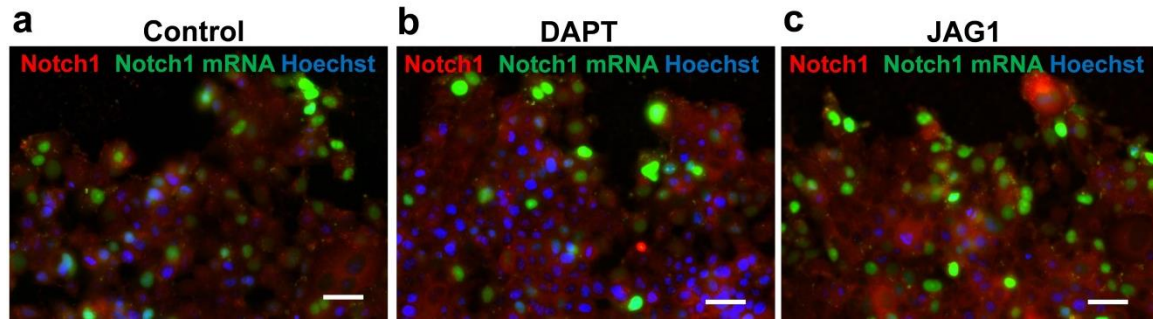
Supplementary Figure 2. Distributions of gene expressions in cells at different locations from the leading edge. (a-d) Intensity distributions of dsLNA probes targeting β -actin mRNA, DII4 mRNA, HO-1 mRNA and random sequence in the first four rows from the leading edge. Each row is approximately 25 μ m in width. Lines serve as visual guides. Over 200 cells were analyzed for each probe. Data are representatives of three independent experiments.



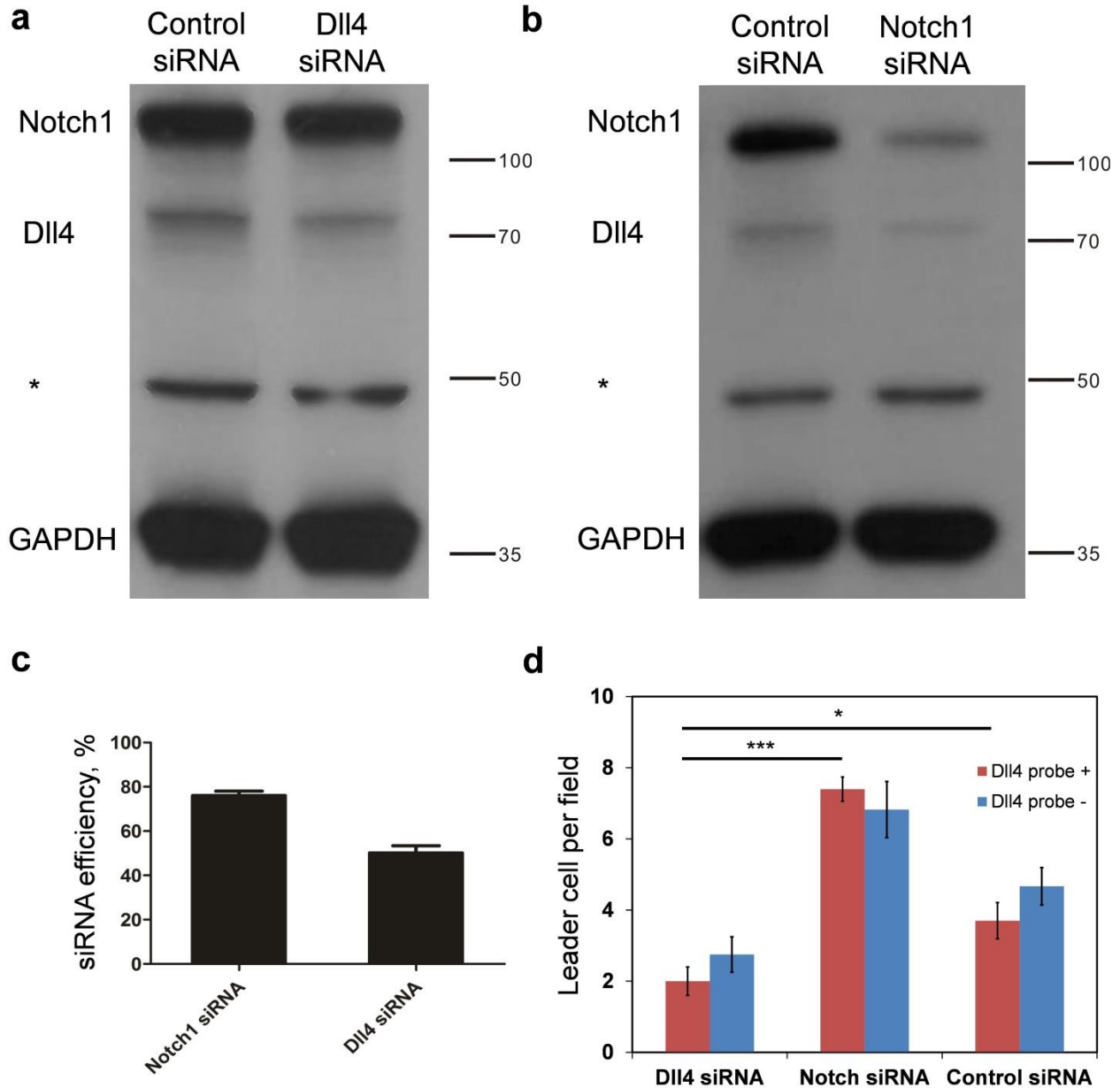
Supplementary Figure 3. Dynamics of leader cell formation during collective cell migration. (a) Time-lapse images illustrating the formation of leader cells after wounding. Examples of leader cells originated from the first row (red arrow) or second row (green arrow) in the boundary. Scale bar, 50 μm . (b) Time-lapse fluorescence images showing the dynamics of Dll4 mRNA expression after wounding. A model wound was created in the top half of the image by scratching the monolayer. The cells could decrease (yellow arrows) or increase (blue arrow) their Dll4 expressions after wounding. Representative images of four independent experiments are shown. Scale bar, 50 μm .



Supplementary Figure 4. Immunofluorescence images of Dll4 and Notch1 in cell monolayers. (a-c) Effects of DMSO (a), DAPT (b) and Jagged-1 (c) treatments on Dll4 and Notch1 expressions. (d-f) Effects of control siRNA (d), Notch1 siRNA (e) and Dll4 siRNA (f) on Dll4 and Notch1 expressions. Representative images of four independent experiments are shown. Scale bars, 50 μ m.

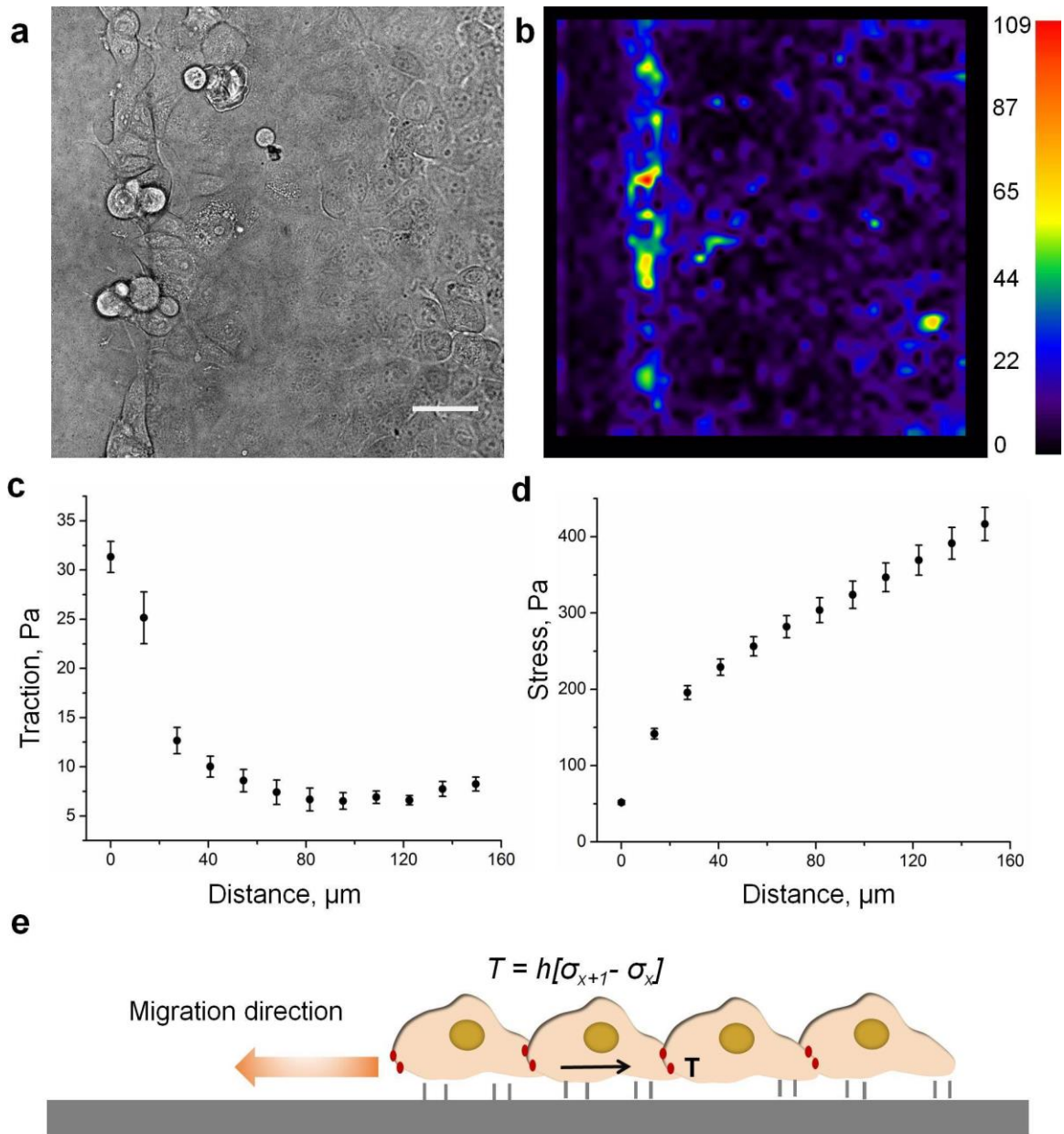


Supplementary Figure 5. Immunofluorescence images of Notch1 and Notch1 mRNA near the boundary. (a-c) Effects of DMSO (a), DAPT (b) and Jagged-1 (c) treatments on Notch1 and Notch1 mRNA expressions. Representative images of three independent experiments are shown. Scale bars, 50 μ m.



Supplementary Figure 6. Characterization of siRNA efficiency. (a-b) Cells were transfected with either scrambled siRNA or siRNA against Notch1 or DII4. Notch1 and DII4 expressions were measured by immunoblotting. The asterisk indicates a non-specific band. (c) Quantification of siRNA efficiency. The siRNA efficiency, represented by the knockdown rate, was $76.0 \pm 3.5\%$ for Notch1 and 50.1 ± 5.7 for DII4. Data

represent mean \pm S.E. of three independent experiments. (d) Effects of Dll4 siRNA and Notch1 siRNA on leader cell density. The experiments were performed in the presence or the absence of the Dll4 dsLNA probe. Data are expressed as mean \pm s.e.m. (n=3, * P < 0.05, *** P < 0.001; unpaired Student's t-test)

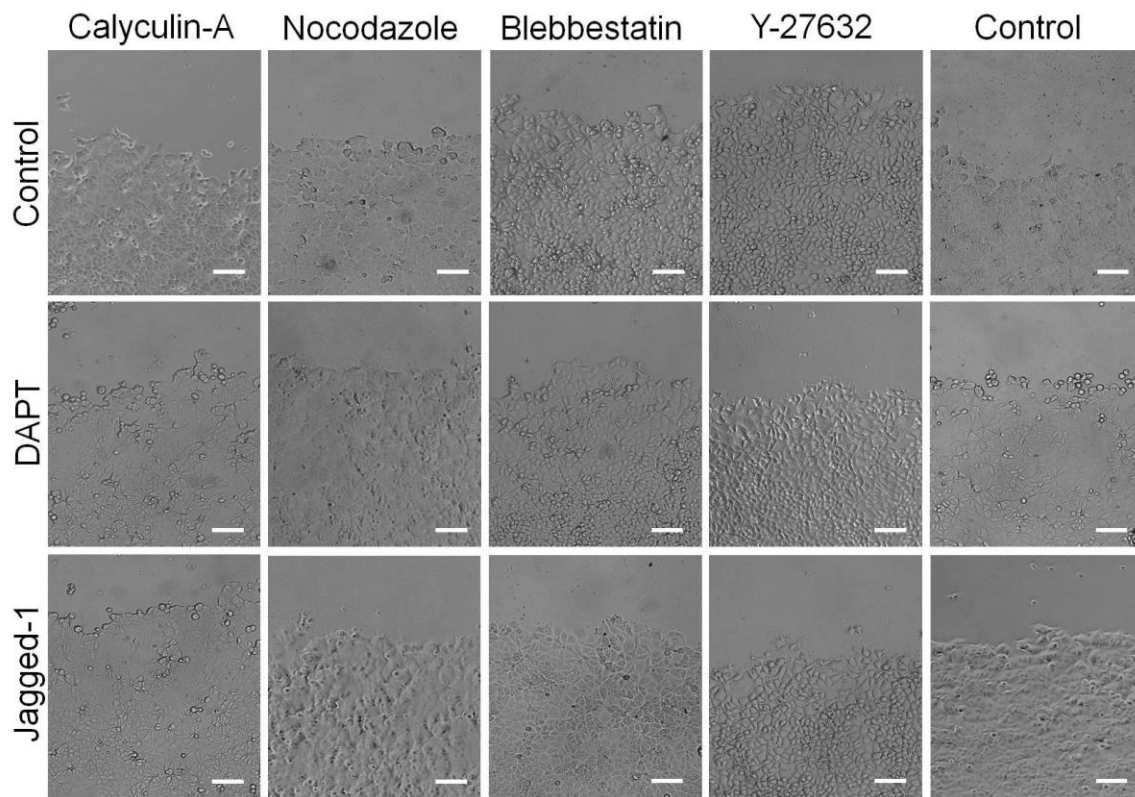


Supplementary Figure 7. Cellular stress distribution near the boundary. (a-b)

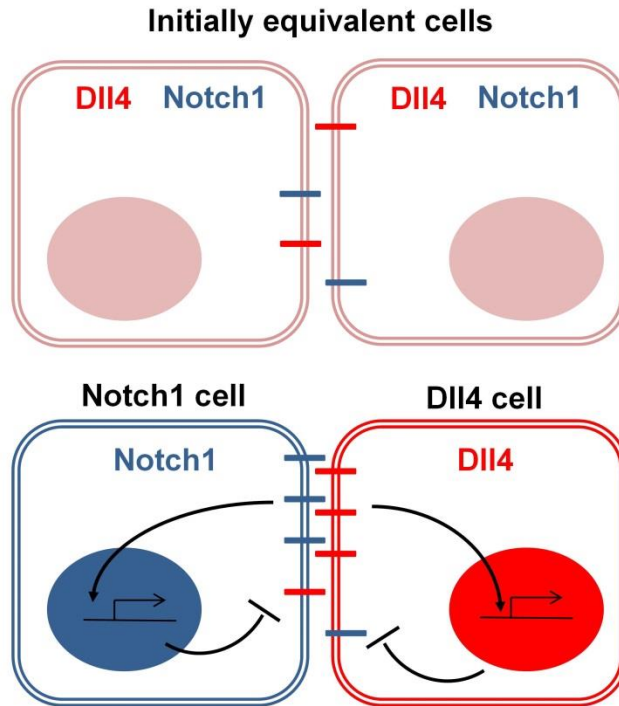
Representative bright-field image (a) and the corresponding traction force distribution (b) of a model wound. The model wound was created by scratching the left hand side of the monolayer. The traction force distribution was obtained using traction force microscopy plugins in ImageJ. The unit of the scale bar is Pascal. Scale bar, 50 μm .

(c) Average normal cell traction force at different positions from the boundary. Data are

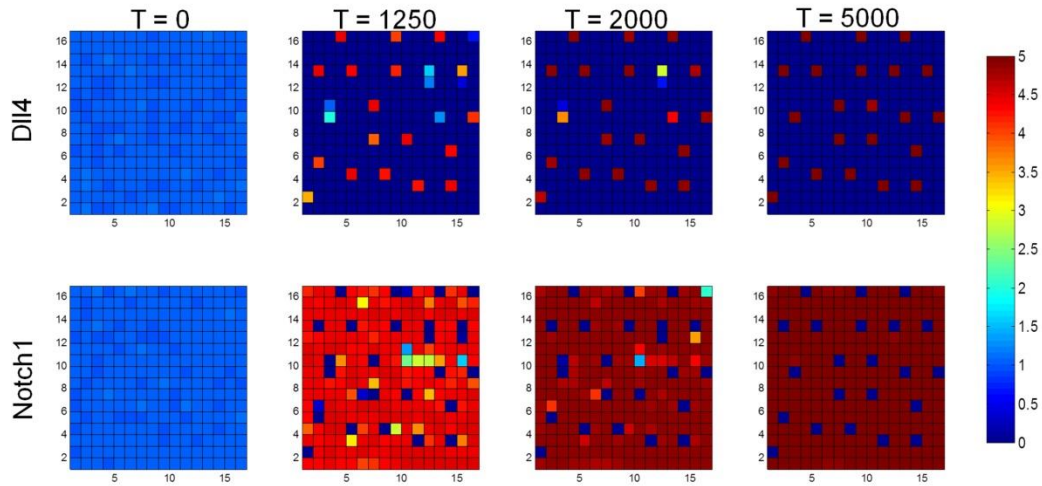
expressed as mean \pm s.d. (n=3). **(d)** Stress distribution within the monolayer as a result of the cumulative cell traction force. Data are expressed as mean \pm s.d. (n=3). **(e)** A tug-of-war model predicting stress accumulation near the leading edge.



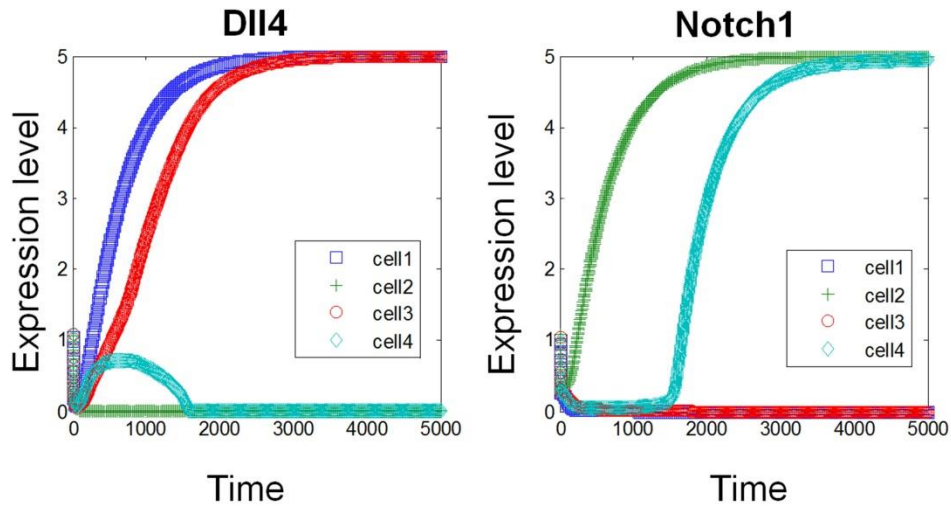
Supplementary Figure 8. Bright-field images of cells treated with cellular force modulating agents (Calycuing-A, Nocodazole, Y-27632, and blebbistatin) and Notch signaling modulating agents (DAPT and Jagged-1). Model wounds were created on the top of the monolayer. Images correspond to the fluorescence images in Fig. 4 of the main text. Scale bars, 100 μ m.



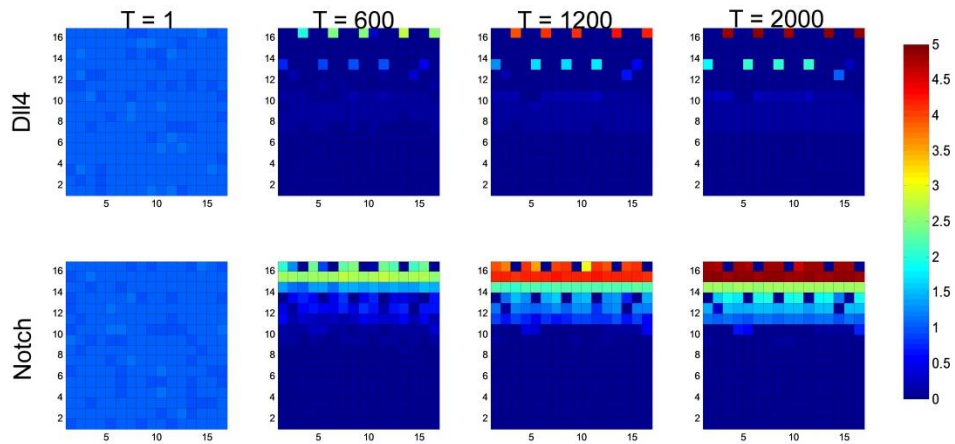
Supplementary Figure 9. Notch1-Dll4 lateral inhibition for cell-fate determination. The cells may initially express the same levels of Notch1 and Dll4. With a small perturbation in the system, the cell with a stronger Dll4 level induces Notch1 activity in the neighboring cell. The neighboring cell increases the Notch activity and decreases the Dll4 level. The Dll4 expressing cell reinforces the expression of Dll4. This results in mutual inactivation of Notch receptor and ligand and cell-fate determination.



Supplementary Figure 10. Dynamics of Notch1-Dll4 lateral inhibition and the formation of checker box patterns. Numerical simulation of Notch1-Dll4 lateral inhibition predicted by equations S1-S3 was performed in a homogeneous cell population with small initial fluctuations. The Dll4 expression is shown in the top row and the corresponding Notch1 expression is shown in the bottom row. Parameters in the simulation are shown in Supplementary Table 3. The computational time scale and the gene expression values are in arbitrary units.



Supplementary Figure 11. Dynamics of Notch1-Dll4 lateral inhibition. Tracking of Notch1 and Dll4 expressions in representative cells. Cells 1 and 2 are adjacent to each other and cells 3 and 4 are adjacent to each other.



Supplementary Figure 12. Numerical simulation of Notch1-Dll4 activity with position dependent expression of Notch1 and Dll4. $L=16$ and $m=3$. All other parameters are the same as Supplementary Table 2.

Supplementary Tables

Supplementary Table 1. Sequences of dsLNA probes with alternating DNA/LNA monomers for single cell gene expression analysis. Bold italic letters represent LNA monomers.

Probe	Name	Sequence & Label	Length (base)
β-actin	Donor (D)	5'-/FAM- 6/AGGAAGGAAGGCTGGAAGAG/-3'	20
	Quencher (Q)	5'-/CTTCCTTCCT/lowa Black FQ/-3'	10
DII4	Donor (D)	5'-/FAM- 6/AAGG GCAG TTGGAGAGGG TT/-3'	20
	Quencher (Q)	5'-/AACTGCCCTT/lowa Black FQ/-3'	10
Notch1	Donor (D)	5'- /FAM6/TGCGGTCTGTCTGG TTGTGC/-3'	20
	Quencher (Q)	5'- ACAGACCGCA/lowa Black FQ/-3'	10
HO-1	Donor (D)	5'-/FAM- 6/AAGACTGGGC TC TCCT TG TT/-3'	20
	Quencher (Q)	5'-/GCCCAG TC TT/lowa Black FQ/-3'	10
Random	Donor (D)	5'-/FAM- 6/ACGC GACAAGCGCACCGATA/-3'	20
	Quencher (Q)	5'-/CTTGTCGCGT/lowa Black FQ/-3'	10

Supplementary Table 2. Sequences of siRNA in this study.

siRNA	Name	Sequence & Label	Length (base)
Notch1	Sense	5'-GGGAC AUCAC GGAUC AUAUT T-3'	21
	Antisense	5'-AUAUG AUCCG UGAUG UCCCG G-3'	21
DII4	Sense	5'-GAGUC UAGUA UUUCA AUAAT T-3'	21
	Antisense	5'-UUAUU GAAAU ACUAG ACUCC A-3'	21

Supplementary Table 3. Parameters in the computational model of Notch1-DII4 lateral inhibition.

Parameters	Symbols	Values
Notch1 expression rate	R_N	0.01
DII4 expression rate	R_D	0.01
Hill coefficient for Notch1	H	3
Hill coefficient for DII4	k	3
Dissociation constant for Notch1	a	0.01
Dissociation constant for DII4	b	100
Notch receptor degradation rate	μ	0.002
Notch ligand degradation rate	P	0.002
Cell contact coefficient	α	0.16
Cis inhibition coefficient	k_c	10

Supplementary Note 1

Notch lateral inhibition. Notch is an evolutionarily conserved intercellular signaling pathway that regulates numerous cell-fate specification events^{1, 2, 3}. Notch receptors and ligands are typically transmembrane proteins and Notch signaling is activated via direct cell-cell contact. One of the key functions of Notch signaling is lateral inhibition, which controls binary cell-fate decision in physically adjacent cells. In Notch lateral inhibition, the expressions of Notch ligands (e.g., Dll4) and receptors (e.g., Notch1) may be similar among the cells initially. With a small difference in Dll4, the cell with a stronger level of Dll4 inhibits the expression of Dll4 in the neighboring cell via Notch1 signaling. Transcriptional feedback amplifies and consolidates the differences between Notch1 and Dll4 expressions, resulting in Notch ligand and receptor expressing cells (Supplementary Fig. 9). The cells may also be under the influence of intrinsic and extrinsic signals in the microenvironment. The mutual inactivation of Notch receptor and ligand can create spatial patterns of cells and controls the proper ratio of specific cell types to regulate the tissue architecture and morphology^{4, 5, 6}. Additional information on Notch signaling can be found from recent review articles.

Computational model of Notch lateral inhibition. Several numerical models have been developed for studying Notch receptor and ligand lateral inhibition. These models have been applied to study numerous developmental events, such as bristle patterning, boundary formation, and angiogenesis sprouting, in both invertebrate and vertebrate species^{4, 5, 6, 7, 8}. We developed a computational model by modifying an established

model of Notch lateral inhibition⁸ to study the formation of leader cell near the boundary. Equations 1-3 show the basic model, which considers the expression of Notch1, N , and Dll4, D . In equation S1, the first term shows the rate of change in Notch1 which is modeled by the Hill equation. This trans-inhibition term depends on the Dll4 level of the neighboring cells, D_{in} . The second term of equation S1 describes the first order degradation of the Notch1. The third term shows the cis-inhibition representing the mutual inactivation of Notch receptor and ligand in the same cell. The cis-inhibition is shown to accelerate patterning dynamics and improve robustness to perturbation⁴. The activity of the Dll4 is modeled similarly by equation S2 except that the expression rate depends on the level of Notch1 in the same cell, effectively implementing the mutual inactivation of Notch1 and Dll4. In equation S3, the immediate and second layers of cells are considered to be in contact to a cell to represent the dynamic filopodial activity of the cells⁸.

$$\frac{dN}{dx} = R_N \frac{D_{in}^k}{a + D_{in}^k} - \mu N - \frac{ND}{k_c} \quad (S1)$$

$$\frac{dD}{dx} = R_D \frac{1}{1 + bN^h} - \rho D - \frac{ND}{k_c} \quad (S2)$$

$$D_{in} = \alpha \sum_{cell \text{ in contact}} D \quad (S3)$$

To study the behaviors of this system, an agent based approach was implemented⁹. In particular, a rectangular array of cells was created to represent the cell monolayer. In each cell, the Notch1 and Dll4 levels, $N(i,j,t)$ and $D(i,j,t)$, were described by equations S1-3, where i and j are position coordinates and t is the time step in the simulation. The equations were discretized in space and time using the finite difference approach and

implemented in MATLAB¹⁰. In the simulation, 16 by 16 elements were considered. For initial conditions, low levels of Dll4 and Notch1 were assigned with small random fluctuations. The model parameters are described in Table N1. Following the original model⁸, the expressions and time scale are expressed in arbitrary units. In the simulation, Notch1-Dll4 lateral inhibition was found to robustly drive the spatial pattern. The system parameters have little effects on the spatial patterns observed. A periodic boundary condition was applied to the monolayer. For wounding, the periodic boundary condition at top edge of the cells was removed to effectively create the boundary.

Notch1-Dll4 lateral inhibition in homogeneous monolayer. The behaviors of the basic model was first studied (Supplementary Fig. 10 and Supplementary Movie 2). Upon the initiation of the simulation, some cells rapidly increased their Dll4 levels while reducing their Notch levels. These Dll4 expressing cells also inhibited the Dll4 levels of neighboring cells. Occasionally, cells with intermediate levels of Dll4 were adjacent to each other, resulting in transient competition of the Dll4 level. Examples of such transient Dll4 competition are shown in Supplementary Fig. 10 (T = 1250, light blue and orange cells). However, the transient competition was not stable. Only one cell “won” the competition and emerged to be the Dll4 expressing cell. The neighboring cells eventually reduced the Dll4 level and expressed a high level of Notch1. The inhibition of Dll4 activity in neighboring cells resulted in the checkbox pattern with approximately equal spacing between the Dll4 expressing cells.

Examining the activities of individual cells further illustrates the dynamic behaviors of Notch1-Dll4 lateral inhibition. Supplementary Fig. 11 shows typical behaviors observed

in the numerical simulation. In particular, most cells rapidly emerged to either high levels of Dll4 or Notch1 (cells 1 and 2 in Supplementary Fig. 11). Cells with intermediate activities were observed to complete for the Dll4 activity (cells 3 and 4 in Supplementary Fig. 11). These behaviors are consistent with our experimental observations (see Fig. 2).

Spatial distribution of Notch1-Dll4 activity near the boundary. The Notch1-Dll4 lateral inhibition model correctly predicted the regular spacing between the leader cells and the dynamic competition of Dll4 activities in adjacent cells. Nevertheless, the checker box pattern observed in the basic model with homogeneous cell distribution did not fully describe the experimental observations. As shown by the dsLNA probe and immunostaining, leader cells were only initiated near the leading edge and the Notch1 expression was upregulated in a region $\sim 300 \mu\text{m}$ near the boundary. The creation of a boundary by removing the periodic boundary condition only induced a small number of leader cells at random positions near the boundary (data not shown). Therefore, additional regulatory signals are likely involved in controlling the formation of leader cells. Specifically, it is known that cells exhibit a gradient in response to the model wound and express various genes in a spatiotemporal manner¹¹. We therefore modify the basic model by incorporating position dependence in Notch1-Dll4 interaction near the boundary. Mathematically, the rate constants, R_N and R_D , were replaced by $R_N(x) = R_N \left(\frac{L-x}{L}\right)^m$ and $R_D(x) = R_D \left(\frac{L-x}{L}\right)^m$ to implement the position dependence. In the rate equations, x is the position of the cell from the leading edge and L is the characteristic length. The exponent, m , represents the slope of the gradient in response. Supplementary Fig. 12 shows the behavior of this spatial model with $m = 3$

and $L = 16$. In this model, the formation of Dll4 expressing leader cells was only observed near the leading edge (i.e., the top boundary). The model also correctly describes the spatial distribution of Notch1 near the boundary. To study the effects of traction force on Dll4 activity, m was chosen from 1, 3, and 5, which effectively modulates the force distribution. To study the effects of Notch signaling, the cell contact coefficient was adjusted between 0.04, 0.16, and 0.32.

Supplementary References

1. Fortini ME. Notch Signaling: The Core Pathway and Its Posttranslational Regulation. *Dev Cell* **16**, 633-647 (2009).
2. Artavanis-Tsakonas S, Rand MD, Lake RJ. Notch signaling: Cell fate control and signal integration in development. *Science* **284**, 770-776 (1999).
3. Bray SJ. Notch signalling: a simple pathway becomes complex. *Nat Rev Mol Cell Biol* **7**, 678-689 (2006).
4. Sprinzak D, *et al.* Cis-interactions between Notch and Delta generate mutually exclusive signalling states. *Nature* **465**, 86-U95 (2010).
5. Sprinzak D, Lakhanpal A, LeBon L, Garcia-Ojalvo J, Elowitz MB. Mutual Inactivation of Notch Receptors and Ligands Facilitates Developmental Patterning. *Plos Comput Biol* **7**, (2011).

6. Shaya O, Sprinzak D. From Notch signaling to fine-grained patterning: Modeling meets experiments. *Curr Opin Genet Dev* **21**, 732-739 (2011).
7. Jakobsson L, *et al.* Endothelial cells dynamically compete for the tip cell position during angiogenic sprouting. *Nat Cell Biol* **12**, 943-953 (2010).
8. Cohen M, Georgiou M, Stevenson NL, Miodownik M, Baum B. Dynamic Filopodia Transmit Intermittent Delta-Notch Signaling to Drive Pattern Refinement during Lateral Inhibition. *Dev Cell* **19**, 78-89 (2010).
9. Long J, Junkin M, Wong PK, Hoying J, Deymier P. Calcium Wave Propagation in Networks of Endothelial Cells: Model-based Theoretical and Experimental Study. *Plos Comput Biol* **8**, e1002847 (2012).
10. LeVeque RJ. *Finite difference methods for ordinary and partial differential equations : steady-state and time-dependent problems*. Society for Industrial and Applied Mathematics (2007).
11. Riahi R, *et al.* Single cell gene expression analysis in injury-induced collective cell migration. *Integrative biology : quantitative biosciences from nano to macro* **6**, 192-202 (2014).